

Evidence for electro-induced membrane defects assessed by lateral mobility measurement of a GPI anchored protein

Jean Michel Escoffre¹, Marie Hubert¹, Justin Teissié¹,
Marie Pierre Rols¹ and Cyril Favard²

¹ Institut de Pharmacologie et de Biologie Structurale,
CNRS UMR 5089, 31077 Toulouse Cedex, France

²Institut Fresnel, CNRS UMR 6133, 13397 Marseille Cedex, France

Submitted to Eur. Biophys. J. 29/11/2013

Abstract

Electrotransfer is a method by which molecules can be introduced in living cells through plasma membrane electropermeabilization. Here, we show that electropermeabilization affects the lateral mobility of RAE-1, a GPI anchored protein. Our results suggest that 10 to 20 % of the membrane surface is occupied by defects or pores and that these defects propagate rapidly (<1 min) over the cell surface. Plasmid DNA (pDNA) electrotransfer also affects the lateral mobility of RAE-1. Furthermore, we clearly show that once inserted into the plasma membrane, pDNA is totally immobile and excludes RAE-1, indicating that pDNA molecules are tightly packed together to form aggregates at least in the outer leaflet of the plasma membrane.

1 Introduction

The permeability of a cell membrane can be transiently increased by applying external electric field pulses. This phenomenon, called electropermeabilization or electroporation, leads to the formation of "membrane defects" or "electropores" in the cell membrane (Neumann et al, 1989; Chang et al, 1992; Weaver, 1993). Since it is an elegant way to introduce exogenous molecules into the cytoplasm, this method is routinely used in basic research, as a very efficient way for the delivery of drugs, oligonucleotides and plasmids (pDNA) but also in-vivo for clinical applications (Mir et al, 2006;

Daud et al, 2008; Low et al, 2009; Escoffre and Rols, 2012; Weiland et al, 2013). Electroporation is a multi-step process occurring on different time scales (Teissie et al, 2005):

1. *Induction step (ns)*. The electric field induces the membrane potential difference to increase. When it reaches a critical value (about 200 mV) local transient permeant structures appears.
2. *Expansion step (μ s)*. Defects expand as long as the field, above the critical value, is present.
3. *Stabilisation step (ms)*. As soon as the field intensity is lower than the critical value, a stabilisation process takes place within a few milliseconds, which brings the membrane to the "permeabilized state".
4. *Resealing step (s, min)*. A slow resealing of the defects is then occurring.
5. *Memory effect (h)*. Some changes in the membrane properties remained present on a longer time scale but the cell behavior is finally back to normal.

If the kinetics of electroporation seems to be well established, very few is known about the changes occurring at the cell and membrane molecular levels (Teissie et al, 2005). Nevertheless, although structural changes in the plasma membrane (i.e., formation of "membrane defects" or "electropores") have never been directly visualized under the microscope, other techniques have been used to observe electroporation. These include measurements of conductivity of cell suspensions and pellets (Kinosita and Tsong, 1979; Abidor et al, 1994; Pavlin et al, 2005, 2007), electro-optical relaxation experiments on lipid vesicles (Kakorin et al, 1996; Griesse et al, 2002), charge pulse studies on lipid bilayers (Griesse et al, 2002; Benz et al, 1979), measurements of membrane voltage on cells with potentiometric fluorescence dyes (Hibino et al, 1993), and monitoring the influx or efflux of molecules and fluorescent dyes (Gabriel and Teissie, 1997, 1999; Pucihar et al, 2008; Rols and Teissie, 1998; Mir et al, 1988; Tekle et al, 1994; Prausnitz et al, 1994, 1995). More recently, molecular simulation on pure lipid models showed the possibility of pore formation during the pulse and pore evolution up to tenth of ns time scale (Levine and Vernier, 2010; Tarek, 2005; Tieleman, 2004). Finally, numerical computation of the evolution of these pores has authorized a more sophisticated, but still theoretical, description of the phenomenon (Krassowska and Filev, 2007). On pure lipid

models, Krassowka et al. predict mean size of "small" pores to be around 1 nm for 97% of them while mean size of "large" pores was around 20 nm with some of them as big as 400 nm on 50 μm vesicles pulsed with a 0.6 kV.cm^{-1} electric field intensity for 1 ms. While small molecules (i.e., < 4 kDa) cross the permeabilized cell membrane directly mainly by post-pulse diffusion, plasmid DNA (pDNA) first interact with the electropermeabilized part of the membrane as shown by the formation of localized aggregates (Escoffre et al, 2011; Pucihar et al, 2008). Taken into account the size of the pDNA (i.e., 3 MDa, 30 nm in diameter) and the negative charges of pDNA (as dielectric exclusion must also be overcome) and supposing that the permeabilization is due to conducting defects called "pores", then these membrane structures must be large and stable (Parsegian, 1969). Nevertheless, since the cell membrane has a much more complex organization than a model lipid bilayer, one expects that the location of regions where pDNA electrotransfer occurs, will be determined not only by the local electric field but also by the local membrane composition and tension (Rosazza et al, 2011). In order to sense the effect of electropermeabilization on the plasma membrane, in the absence or presence of pDNA, we have monitored the lateral mobility of a GPI anchored protein Rae-1 during the resealing step, by means of fluorescence recovery after photobleaching (FRAP) experiments. As a GPI anchored, Rae-1 (MHC-I homologous protein) is located in the outer leaflet of the plasma membrane without any partitioning into lipid domains previously described (Nomura et al, 1996; Zou et al, 1996). Therefore GPI anchored has been considered as a good candidate to report changes in the plasma membrane lateral state and in its close interface with the outside of the cell. By measuring its mobility before and after application of permeabilizing electric field pulses in absence of pDNA, we reported a drastic and significant increase of the half-time of fluorescence recovery and a decrease of the mobile fraction, both at the anode and cathode facing pole of the cell. These experimental data are in favor of the creation of obstacles in the plasma membrane (e.g., "pores", "membrane defects"). We then showed that when pDNA is inserted into the membrane after electropermeabilization, Rae-1 is totally unable to re-enter the area occupied by pDNA, confirming the direct observation that pDNA is accumulated in a tightly bound manner into clusters.

2 Material and Methods

2.1 Expression of Rae-1 in CHO cell line

The eGFP-Rae-1 CHO cells have been generously made by Dr. B. Couderc (EA3035, Institut Claudius Regaud, France). CHO cells have been transfected by pDNA encoding Rae1-eGFP fusion protein (generous gift from Dr. A. Aucher and Dr. D. Hudrisier, IPBS-CNRS, UMR5089, France). The transfected cells are cultured under selective pressure with G418 ($1 \mu\text{g}/\mu\text{L}$) (InvivoGen, San Diego, CA). The eGFP-Rae-1 expressing cells were sorted out by flow cytometry (FAScan; Beckman. Instruments, Inc. Fullerton, CA). Cells were then grown as previously described (Phez et al, 2005).

2.2 pDNA labeling for electroporation

4.7-kbp plasmid (pEGFP-C1, Clontech, Palo Alto, CA) carrying the green fluorescent protein gene controlled by the CMV promoter was prepared from *Escherichia coli* transfected bacteria by using Maxiprep DNA purification system (Qiagen, Chatsworth, CA, USA). They were covalently labeled with Cy-3 fluorophore using Label-IT nucleic acid labeling kit (Mirus, Madison, WI, USA) according to the manufacturer protocol. The fluorescent labeling did not affect the function of expression cassette.

2.3 Electroporation

Electroporation was carried out with a CNRS cell electropulsator (Jouan, St Herblain, France), which delivers square-wave electric pulses. An oscilloscope (Enertec, St. Etienne, France) was used to monitor the pulse shape. The electroporation chamber was built using two stainless-steel parallel rods (diameter 0.5 mm, length 10 mm, inter-electrode distance 5 mm) placed on a Lab-tek chamber (Mazères et al, 2009). The electrodes were connected to the voltage generator. A uniform electric field was generated. The chamber was placed on the stage of the confocal microscope (Zeiss, LSM 510, Germany). Electroporation of cells was performed by application of millisecond electric pulses, conditions required to efficiently transfer macromolecules such as pDNA into cells (Rols and Teissié, 1998). Ten pulses of 5 ms duration and 0.6 kV/cm amplitude were applied at a frequency of 1 Hz at room temperature. For FRAP experiments, the eGFP-Rae-1 CHO cells were seeded on a microscope glass coverslip chamber (Labtek II system, Nunc™, Denmark) at $0.5 \cdot 10^6$ cells per well 24h before electroporation. Cells were electropulsed in 200 μL of pulsation buffer (10 mM $\text{K}_2\text{HPO}_4/\text{KH}_2\text{PO}_4$, 1

mM MgCl₂, 250 mM sucrose, pH 7.4). In absence of pDNA, the cell electropermeabilization was monitored by adding propidium iodide at 100 μ M in the pulsation buffer. Eighty percent of cells located between the electrodes were permeabilized. The cell electropermeabilization in presence of Cy3-pDNA was performed after adding of 2 μ g of Cy3-pDNA in 200 μ l of pulsation buffer. Cy3-pDNA molecules interacted with more than 60% of cells located between the electrodes.

2.4 Fluorescence recovery after photobleaching

FRAP experiments were conducted using a Zeiss LSM-510 confocal microscope. The image sequence was acquired at a 5 Hz frequency using the 488 nm line of an argon ion laser at a very low power to avoid photobleaching during recording. After 50 images, 4 regions of interests (ROI), of 1 μ m radius each, which correspond to 0.86 μ m waist of a Gaussian beam, located in front of anode and cathode respectively and on left and right sides of the cell (see 3.1 for illustration), were rapidly photobleached ($t < 300$ ms) at maximal laser power. Fluorescence recovery was monitored by acquiring successive images during 40 s. The recovery curves were obtained by plotting the mean fluorescence intensity as a function of time in these two ROI, and were corrected for fluctuations in axial position by a third ROI located into the cell, and finally normalized to the mean value of each ROI before photobleaching. The curves were fitted using Eq.1 which is a slightly modified 2D diffusion model for FRAP taking into account normalization and a mobile fraction M (Axelrod et al, 1976; Matthews and Favard, 2007):

$$F(t) = M \sum_{n=1}^{\infty} \frac{(-K)^n}{n!} \frac{1}{1 + n + 2n \frac{t}{t_{1/2}}} + (1 - M)F_0 \quad (1)$$

This equation was used to its 20th order limited development for data fitting. Fluorescence recoveries were acquired before electric pulses and at a time t , 30 s $< t < 90$ s after electropermeabilization on the same sample using the same sequence. At this time t , more than 50% of the cells were still permeabilized (Rols and Teissié, 1998).

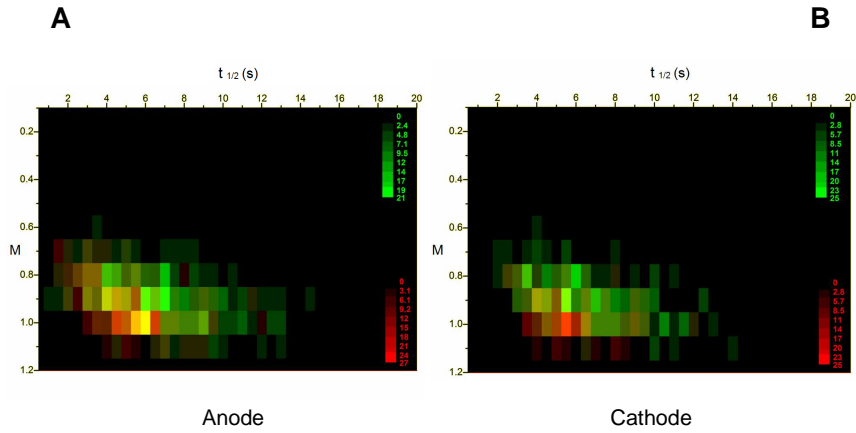


Figure 1: **Distribution of $t_{1/2}$ and M before and after electropermeabilization:** M was plotted as a function of $t_{1/2}$, before (in red) and after (in green) electropermeabilization for the cell pole facing the anode (A), or the cathode (B). Intensity scale is dispatched on the side of each image and correspond to the number of events in each class of $(t_{1/2}, M)$ pair.

3 Results

3.1 Effects of electropermeabilization on the mobility of Rae-1 protein

Mobility of Rae-1 protein was monitored by means of FRAP experiments. Fitting of the recovery curve using equation 1 lead to determination of two different parameters which are respectively : $t_{1/2}$ which is the half-time of recovery and M which is the mobile fraction. $t_{1/2}$ is a function of the diffusion coefficient of Rae-1 protein, the second one is a function of the number of mobile Rae-1 protein. In order to analyze the mobility of Rae-1 molecule, the mobile fraction was plotted as a function of the half-time of recovery at the anode (Figure 1A) and the cathode (Figure 1B) before (in red) and after (in green) electropermeabilization, for a set of 250 different cells. The intensity of each pixel represents the number of events belonging

to each class.

		n	$t_{1/2}$ (s)	p-value	M	p-value
Anode (1)	before EP	436	5.4 ± 2.3	$< 10^{-4}$	0.88 ± 0.10	7.10^{-4}
	after EP		7.0 ± 3.2		0.86 ± 0.09	
Cathode (2)	before EP	459	5.6 ± 2.6	$< 10^{-4}$	0.89 ± 0.09	$< 10^{-4}$
	after EP		6.9 ± 3.2		0.85 ± 0.10	
Left (3)	before EP	315	5.3 ± 1.8	$< 10^{-4}$	0.91 ± 0.08	$< 10^{-4}$
	after EP		6.2 ± 2.2		0.85 ± 0.09	
Right (4)	before EP	316	5.8 ± 1.8	$< 10^{-4}$	0.93 ± 0.08	$< 10^{-4}$
	after EP		6.7 ± 2.3		0.90 ± 0.09	

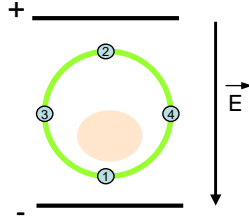


Table 1: Mean values of $t_{1/2}$ and M before and after permeabilization and their respective paired t-test values and localization of the measurements in cell. Localization of the experimental positions are depicted on the scheme of the cell below the table.

As described in Figure 1, the mobility of Rae-1 protein is reduced on both sides of the cell facing the electrodes (i.e., anode and cathode) after electropermeabilization (M slightly decreases and $t_{1/2}$ increases). The mean values and standard deviations of $t_{1/2}$ and M, at the pole of the cell facing the anode and the cathode, before and after electropermeabilization, as well as the left and right part of the equatorial level of the cell (perpendicular to the electric field direction) are reported in the Table 1 using descriptive statistics. Student's t-tests has been performed on paired values of cathode and anode showing that both parameters scored $p < 0.001$ and can be considered as significantly different before and after electropermeabilisation. Interestingly, an increase in the of $t_{1/2}$ and a decrease of M has also been observed in the membrane regions not facing the electrodes.

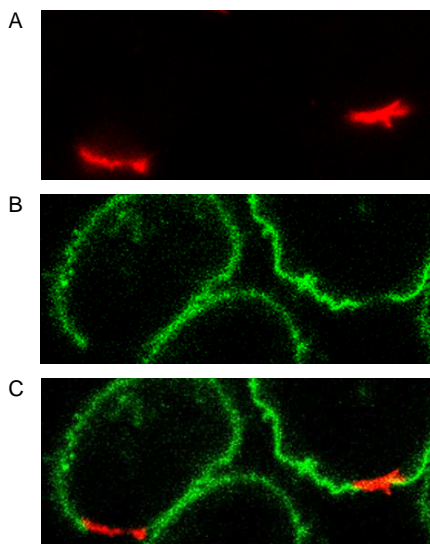


Figure 2: Images of GFP-Rae-1 and Cy3-pDNA after electroinsertion of Cy3-pDNA: Cy3-pDNA is located at the pole of the cells immediately after the end of electropulsation (part A), covering large area at the cell surface. Fluorescence of GFP-Rae1 is located at the plasma membrane of the CHO cells (part B) but is clearly extinguished in the area occupied by Cy3-pDNA. This is confirmed by merging the two images (part C) where no colocalization can be seen.

3.2 Effects of pDNA electroinsertion on the mobility of Rae-1 protein

Photonic microscopy observations of gene electrotransfer process reveals that pDNA molecules are found as clusters with an apparent size close or above diffraction limit i.e. 200 nm (Golzio et al, 2002). We attempted to probe the size of these pDNA clusters more accurately by using Rae-1 dynamics. An effect on mobility of the protein may occur since mobility is reduced by the presence of obstacles and this reduction is proportional to the size and density of obstacles. Unfortunately, direct image analysis of eGFP-Rae-1 expressing cells showing an electroinsertion of Cy3-pDNA revealed that Rae-1 fluorescence was excluded from the Cy3-pDNA cluster avoiding any possibility to perform FRAP measurements (Figure 2). Nevertheless, absence of measurable fluorescence does not directly mean absence of Rae-1 proteins. Indeed, since emission spectrum of eGFP widely overlaps absorption spectrum of Cy3, lack in fluorescence can be due to a very efficient

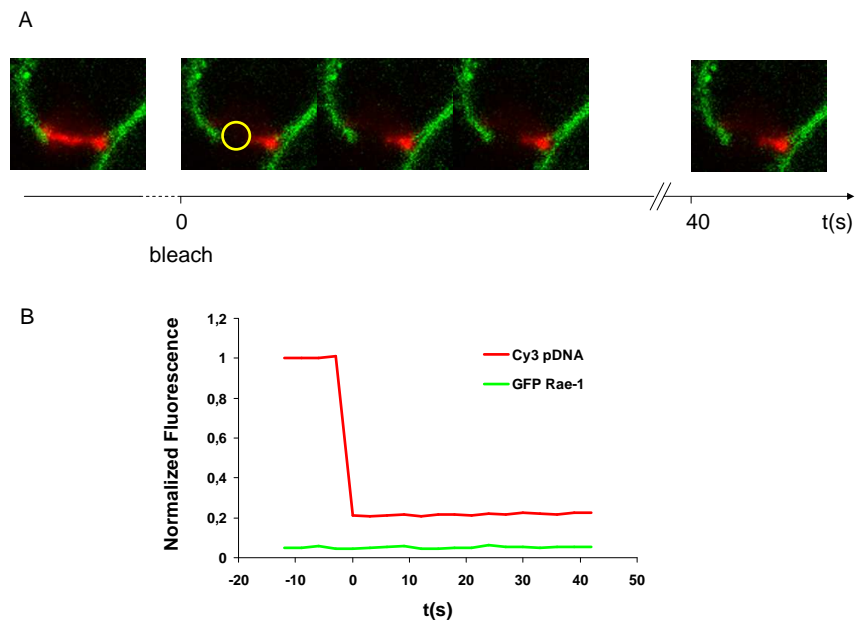


Figure 3: Photobleaching of Cy3-pDNA after electroinsertion. In Part A are represented images of Cy3-pDNA (in red) and GFP-Rae-1 (in green) fluorescence acquired during the expected recovery process. The photobleached area is located inside the yellow circle. In Part B is shown the fluorescence intensities integrated in the yellow circle of Cy3-pDNA (in red) and GFP-Rae-1 (in green) normalized to the value of Cy3-pDNA before the bleaching. These two curves clearly show that fluorescence recovery occurred neither for Cy3-pDNA, nor for eGFP-Rae-1, leading to the conclusion that the Cy3-pDNA is highly immobile and that Rae-1 is totally excluded from the Cy3-pDNA clusters located in the membrane.

energy transfer of Perrin-Forster type from eGFP to Cy3. Therefore, as shown in Figure 3, photobleaching FRET experiments were performed. The Cy3-pDNA was photobleached using the 546 nm line of an He-Ne laser on the confocal microscope. Occurrence of FRET should result in an increase in the fluorescence of eGFP-Rae-1 protein (Figure 3 part B, green line). This was not the case, indicating that no FRET occurred between Cy3-pDNA and eGFP-Rae-1 protein. More interestingly, the time evolution of the experiment immediately after the bleaching, up to 42 s after (40 s being the total time of acquisition in FRAP experiments of section 3.1) showed no recovery neither for Cy3-pDNA (Figure 3 part B, red line), nor for eGFP-Rae-1 protein, confirming a total absence of mobility of Cy3-pDNA and indicating a total inaccessibility of eGFP-Rae-1 into these clusters.

4 Discussion

4.1 Macroscopic effects of electropermeabilization.

Figure 4 illustrates how the osmotic swelling can locally change the tension of plasma membrane. The FRAP recovery half-time is the time needed for the molecule to explore the mean square of a length defined by the waist of the laser. When applied to measurement of lateral diffusion in cell plasma membrane, this definition assumes that the plasma membrane is perfectly flat and perpendicular to the laser path. While swelling will not affect the angle of intercept of the laser and the plasma membrane it can dramatically change the flatness of the plasma membrane (this latter becoming flatter than before swelling). Therefore, if a molecule diffuses with the same diffusion coefficient before and after electrically-mediated swelling, it will take less time to recover fluorescence in a tensed situation (closer to the real waist) than in a loose situation (further from the real waist). Our results here show exactly the opposite effect, emphasizing the existence of microscopic obstacles to free diffusion after electropermeabilization. Moreover, our study shows that these obstacles are also present at the equator of the cell (i.e. locations parallel to the electrodes) one minute after electropermeabilization. This unexpected result proves that these obstacles are a collective signal all around the cell. This is confirmative, but with a much faster time resolution, of the recent work of Chopinet et al. (Chopinet et al, 2013) that evidenced on living CHO cells a rapid propagation of membrane perturbation along the entire cell surface using AFM imaging.

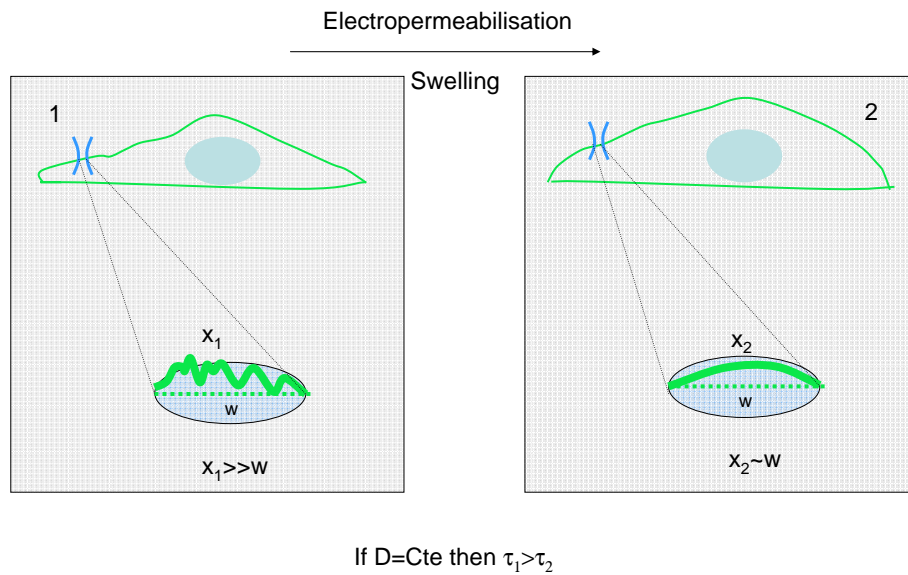


Figure 4: Incidence of the cell swelling induced by electropermeabilization on the estimation of recovery time in FRAP experiments: This scheme depicts the effect of cell swelling induced by electropermeabilization (from 1(left) to 2(right)). The swelling ends in a more tensed membrane as compared to the resting cell. Since the laser waist is constant and assuming that the axis of the laser is kept normal to the plane of the membrane, it can be seen from this scheme that the area analysed during FRAP experiments is lower after swelling than before. Therefore, without any change in diffusion constant of the observed molecule, the recovery time after electropermeabilization will be lower than before.

4.2 Change in the mobility of Rae-1 : relation to the permeabilized area.

Saxton (Saxton, 1982, 1987) has theoretically showed that apparent diffusion coefficient of a tracer decrease with the fractional area occupied by obstacles, down to zero if obstacles are immobile at a given area (i.e., the percolation threshold), or asymptotically if obstacles are very mobile (as compared to the tracer), meaning that no more percolation threshold exist. In this study, apparent diffusion coefficient (i.e. half-time recoveries at constant given waists) of eGFP-Rae-1 protein is decreased as much as 10% after electroporation. This result is a confirmation of the existence of "defects" at least in the outer leaflet of the plasma membrane, since the tracer, eGFP-Rae-1 protein is located in this leaflet. This confirms previous results obtained by other approaches such as influx of fluorescent dyes into the cytosol (Gabriel and Teissié, 1997, 1999; Pucihar et al, 2008; Rols and Teissié, 1998; Mir et al, 1988; Tekle et al, 1994; Prausnitz et al, 1994, 1995). According to Saxton's numerical simulations, a decrease of 10% of the apparent diffusion coefficient means that 10% (in the case of immobile "pores" or "defects") to 20% (in the case of very fast diffusing "pores" or "defects") of the total membrane area of the cell are occupied by these "defects" or "pores". In order to compare with experimental (Gabriel and Teissié, 1997, 1999; Tekle et al, 2001; Portet et al, 2011) or numerical simulation (Krasowska and Filev, 2007) data available in the literature, we have defined an aperture angle ($0 < \theta_{ap} < 90^\circ$) of permeabilisation as the half angle of the solid angle in which the total permeabilized surface is included. In this work, if all the obstacles were fused in a unique one, this aperture angle will be found between 36° and 52° . Portet et al. measured the average aperture angle of pores to be 6° by using pDNA translocation into giant unilamellar vesicles (GUVs) made of DOPC. Using GUVs made of DOPC with a radius close to the CHO cells (i.e., $15 \mu\text{m}$) and electric fields twice our value (1.2 kV.cm^{-1}), Tekle et al. (Tekle et al, 2001) shown that up to 14% of the total membrane surface can be lost when pulsing, leading to a value of 44° . Finally, Gabriel et al. (Gabriel and Teissié, 1999) measured the average aperture angle as the angle of the extent of the permeabilization immediately after the pulse by visualizing small fluorophore entrance into the cell to be 56° . θ_{ap} values found from these different studies exhibit discrepancies. Many factors can account for that discrepancies amongst, which the duration and the strength of the external applied electric field, differences in model used (cells (Gabriel and Teissié, 1999, 1997) or artificial lipid membranes (Tekle et al, 2001; Portet et al, 2011)) in their radius or in the case of differences in

external and internal buffers used for electropermeabilization. Nevertheless in (Gabriel and Teissié, 1999) the results have been obtained using exactly the same experimental conditions than ours (i.e., cell type, electropermeabilization buffer and electric field intensity range) and can therefore be directly compared. These results exhibit a value of θ_{ap} slightly superior to what is found here. Indeed, lifetime distribution of "pores" or "defects" in lipid membranes spans a wide range between microseconds up to minutes depending on several factors (e.g., field intensity, conductance, lipid membrane composition, artificial vesicles or cells) (Teissie et al, 2005). However, it is clear that the number and/or size of the "pores" decreases with time after electropermeabilization. Since our experiments have been conducted one minute at least after the end of pulse sequence, this effect could account for a smaller value of θ_{ap} as compared to the one found in (Gabriel and Teissié, 1999, 1997). Alternatively, Krassowska et al. (Krassowska and Filev, 2007) performed numerical simulation of the evolution in time and space of pores in a spherical pure lipid vesicle exposed to an electric field. They simulated the normalized average area occupied by these "pores" as a function of the external electric field applied to the cell. For an electric field use in this study of 0.2 kV.cm^{-1} (that corresponds to our conditions regarding the $50 \text{ }\mu\text{m}$ radius they use in their simulations) they found this area to be 0.07% of the total area ($=1^\circ$) which is far beyond our experimental results. Nevertheless, their values were obtained using only one pulse of 1 ms. If one makes this oversimplified hypothesis that the number and therefore the area occupied by the "pores" is a function not only of the electric field intensity, but also of the total exposure time of cell to an electric field. Furthermore, if one admits that the created "pores" in each impulsion do not reseal during our total pulse sequence, the area occupied by the pores should be 50 times more important than in their study, resulting in an apparent angle of ($=23^\circ$) which is closer to what we find here.

4.3 Effect of pDNA electroinsertion on the lateral mobility of Rae-1.

The apparent size of the pDNA clusters inserted into the membrane after electropermeabilization (larger than 200 nm in diameter, (Golzio et al, 2002; Phez et al, 2005)) should lead to a drastic increase in the half-time recovery ($t_{1/2}$) and a drastic decrease in the mobile fraction (M) due to eGFP-Rae-1 proteins trapped in this pDNA clusters. Unfortunately the very low level or the total absence of fluorescence of Rae-1 in the pDNA clusters at the membrane did not permit to perform efficient FRAP measurements.

This absence of fluorescence could be of two different origins :

- Loss in fluorescence of the eGFP-Rae-1 protein due to very efficient energy transfer of Perrin-Förster type (FRET) between eGFP fused Rae-1 protein and Cy-3 labeling the pDNA.
- Exclusion of Rae-1 molecules from the pDNA clusters.

Photobleaching FRET experiments have been performed in order to discriminate between these two possibilities. The absence of recovery in the fluorescence of Rae-1 proteins when the Cy-3 molecules are bleached clearly shows that eGFP-Rae-1 proteins are totally excluded from pDNA clusters induced by electroporation. On the other hand, no recovery occurs for pDNA fluorescence, confirming that the pDNA clusters are highly immobile, as previously described (Escoffre et al, 2011). This result is in favor of a pDNA aggregate that excludes some of the membrane components, if not all, to its periphery.

5 Conclusion

In order to sense at the molecular scale the effect of electroporation and pDNA electroinsertion on the plasma membrane lateral organization, mobility of a tracer (Rae-1 protein) has been assessed in living cells. This study shows that membrane reporters can sense the defects induced by electroporation and estimate correctly the surface permeabilized during field exposure. More interestingly, this study shows that these defects can propagate rapidly all over the surface of the plasma membrane. The local creation of a permeabilized cap on the cell surface triggers a global cellular effect. Finally, attempting to perform such an approach to characterize the nature of pDNA clusters immediately after electroinsertion, we have shown that these clusters were highly dense since they did not allow Rae-1 protein to penetrate into them.

6 Acknowledgements

This work has been performed in collaboration with the "Toulouse Réseau Imagerie" core IPBS facility (Genotoul, Toulouse, France), which is supported by the Association Recherche Cancer, Region Midi Pyrenees, the European union (FEDER) and Grand Toulouse cluster. This research project was conducted in the scope of EBAM European Associated Laboratory and of the COST Action TD1104. JM Escoffre was

the recipient of an allocation de recherche du Ministère de l'Enseignement Supérieur et de la Recherche. The authors are grateful to Dr. M. Golzio for critical reading of the manuscript. C. Favard is a membership of CNRS consortii GDR2588 "MIV" and GDR3070 "CellTiss".

References

- Abidor IG, Li LH, Hui SW (1994) Studies of cell pellets: II. osmotic properties, electroporation, and related phenomena: membrane interactions. *Biophys J* 67(1):427–435
- Axelrod D, Koppel D, Schlessinger J, Elson E, Webb W (1976) Mobility measurement by analysis of fluorescence photobleaching recovery kinetics. *Biophys J* 16(9):1055–1069
- Benz R, Beckers F, Zimmermann U (1979) Reversible electrical breakdown of lipid bilayer membranes: a charge-pulse relaxation study. *J Membr Biol* 48(2):181–204
- Chang D, Chassy B, Saunders J, Sowers A (1992) *Guide to Electroporation and Electrofusion*. San Diego
- Chopinet L, Roduit C, Rols MP, Dague E (2013) Destabilization induced by electropermeabilization analyzed by atomic force microscopy. *Biochim Biophys Acta* 1828(9):2223–2229
- Daud AI, DeConti RC, Andrews S, Urbas P, Riker AI, Sondak VK, Munster PN, Sullivan DM, Ugen KE, Messina JL, Heller R (2008) Phase I trial of interleukin-12 plasmid electroporation in patients with metastatic melanoma. *J Clin Oncol* 26(36):5896–5903
- Escoffre JM, Rols MP (2012) Electrochemotherapy: Progress and prospects. *Curr Pharm Des*
- Escoffre JM, Portet T, Favard C, Teissie J, Dean DS, Rols MP (2011) Electromediated formation of DNA complexes with cell membranes and its consequences for gene delivery. *Biochim Biophys Acta-Biomembranes* 1808(6):1538–1543
- Gabriel B, Teissie J (1997) Direct observation in the millisecond time range of fluorescent molecule asymmetrical interaction with the electropermeabilized cell membrane. *Biophys J* 73(5):2630 – 2637
- Gabriel B, Teissie J (1999) Time courses of mammalian cell electropermeabilization observed by millisecond imaging of membrane property changes during the pulse. *Biophys J* 76(4):2158 – 2165
- Golzio M, Teissie J, Rols MP (2002) Direct visualization at the single-cell level of electrically mediated gene delivery. *Proc Natl Acad Sci U S A* 99(3):1292–1297

- Griese T, Kakorin S, Neumann E (2002) Conductometric and electrooptic relaxation spectrometry of lipid vesicle electroporation at high fields. *Phys Chem Chem Phys* 4(7):1217–1227
- Hibino M, Itoh H, Kinoshita K (1993) Time courses of cell electroporation as revealed by submicrosecond imaging of transmembrane potential. *Biophys J* 64(6):1789–1800
- Kakorin S, Stoylov S, Neumann E (1996) Electro-optics of membrane electroporation in diphenylhexatriene-doped lipid bilayer vesicles. *Biophys Chem* 58(1-2):109–116
- Kinoshita K, Tsong TY (1979) Voltage-induced conductance in human erythrocyte membranes. *Biochim Biophys Acta* 554(2):479–497
- Krassowska W, Filev PD (2007) Modeling electroporation in a single cell. *Biophys J* 92(2):404 – 417
- Levine ZA, Vernier PT (2010) Life cycle of an electropore: field-dependent and field-independent steps in pore creation and annihilation. *J Membr Biol* 236(1):27–36
- Low L, Mander A, McCann K, Dearnaley D, Tjelle T, Mathiesen I, Stevenson F, Ottensmeier CH (2009) DNA Vaccination with Electroporation Induces Increased Antibody Responses in Patients with Prostate Cancer. *Hum Gene Ther* 20(11):1269–1278
- Matthews C, Favard C (2007) Theory, principles and applications of fluorescent technologies in cellular biology and cancer research. *Bull Cancer (French)* 94(1):115–125
- Mazères S, Sel D, Golzio M, Pucihar G, Tamzali Y, Miklavcic D, Teissié J (2009) Non invasive contact electrodes for in vivo localized cutaneous electropulsation and associated drug and nucleic acid delivery. *J Control Release* 134(2):125–131
- Mir L, Banoun H, Paoletti C (1988) Introduction of definite amounts of nonpermeant molecules into living cells after electropermeabilization - direct access to the cytosol. *Exp Cell Res* 175(1):15–25
- Mir LM, Gehl J, Sersa G, Collins CG, Garbay JR, Billard V, Geertsen PF, Rudolf Z, O’Sullivan GC, Marty M (2006) Standard operating procedures of the electrochemotherapy: Instructions for the use of bleomycin or cisplatin administered either systemically or locally and electric pulses delivered by the Cliniporator (TM) by means of invasive or non-invasive electrodes. *EJC Suppl* 4(11):14–25
- Neumann E, Sowers A, Jordan C (1989) *Electroporation and Electrofusion in Cell Biology*

- Nomura M, Zou Z, Joh T, Takihara Y, Matsuda Y, Shimada K (1996) Genomic structures and characterization of rael family members encoding gpi-anchored cell surface proteins and expressed predominantly in embryonic mouse brain. *J Biochem* 120(5):987–995
- Parsegian V (1969) Energy of an ion crossing of a low dielectric membrane: Solutions to four relevant electrostatic problems. *Nature* 221:844–846
- Pavlin M, Kanduser M, Rebersek M, Pucihar G, Hart FX, Magjarevic R, Miklavcic D (2005) Effect of cell electroporation on the conductivity of a cell suspension. *Biophys J* 88(6):4378–4390
- Pavlin M, Leben V, Miklavcic D (2007) Electroporation in dense cell suspension—theoretical and experimental analysis of ion diffusion and cell permeabilization. *Biochim Biophys Acta* 1770(1):12–23
- Phez E, Faurie C, Golzio M, Teissie J, Rols M (2005) New insights in the visualization of membrane permeabilization and DNA/membrane interaction of cells submitted to electric pulses. *Biochim Biophys Acta-Gen Subj* 1724(3):248–254
- Portet T, Favard C, Teissie J, Dean DS, Rols MP (2011) Insights into the mechanisms of electromediated gene delivery and application to the loading of giant vesicles with negatively charged macromolecules. *Soft Matter* 7(8):3872–3881
- Prausnitz MR, Milano CD, Gimm JA, Langer R, Weaver JC (1994) Quantitative study of molecular transport due to electroporation: uptake of bovine serum albumin by erythrocyte ghosts. *Biophys J* 66(5):1522–1530
- Prausnitz MR, Corbett JD, Gimm JA, Golan DE, Langer R, Weaver JC (1995) Millisecond measurement of transport during and after an electroporation pulse. *Biophys J* 68(5):1864–1870
- Pucihar G, Kotnik T, Miklavich D, Teissié J (2008) Kinetics of transmembrane transport of small molecules into electropermeabilized cells. *Biophysical Journal* 95(6):2837 – 2848
- Rols MP, Teissié J (1998) Electropermeabilization of mammalian cells to macromolecules: Control by pulse duration. *Biophysical Journal* 75(3):1415 – 1423
- Rosazza C, Escoffre JM, Zumbusch A, Rols MP (2011) The actin cytoskeleton has an active role in the electrotransfer of plasmid dna in mammalian cells. *Mol Ther* 19(5):913–921
- Saxton M (1982) Lateral diffusion in an archipelago - Effects of impermeable patches on diffusion in a cell-membrane. *Biophys J* 39(2):165–173
- Saxton M (1987) Lateral diffusion in an archipelago - The effect of mobile obstacles. *Biophys J* 52(6):989–997

- Tarek M (2005) Membrane electroporation: a molecular dynamics simulation. *Biophys J* 88(6):4045–4053
- Teissie J, Golzio M, Rols M (2005) Mechanisms of cell membrane electropermeabilization: A minireview of our present (lack of ?) knowledge. *Biochim Biophys Acta - Gen Subj* 1724(3):270 – 280
- Tekle E, Astumian RD, Chock PB (1994) Selective and asymmetric molecular transport across electroporated cell membranes. *Proc Natl Acad Sci U S A* 91(24):11,512–11,516
- Tekle E, Astumian R, Friauf W, Chock P (2001) Asymmetric pore distribution and loss of membrane lipid in electroporated DOPC vesicles. *Biophys J* 81(2):960–968
- Tieleman DP (2004) The molecular basis of electroporation. *BMC Biochem* 5:10
- Weaver J (1993) Electroporation: a general phenomenon for manipulating cells and tissues. *J Cell Biochem* 51:426–435
- Weiland O, Ahlén G, Diepolder H, Jung MC, Levander S, Fons M, Mathiesen I, Sardesai NY, Vahlne A, Frelin L, Sällberg M (2013) Therapeutic dna vaccination using in vivo electroporation followed by standard of care therapy in patients with genotype 1 chronic hepatitis c. *Mol Ther* 21(9):1796–1805
- Zou Z, Nomura M, Takihara Y, Yasunaga T, Shimada K (1996) Isolation and characterization of retinoic acid-inducible cDNA clones in f9 cells: a novel cDNA family encodes cell surface proteins sharing partial homology with MHC class I molecules. *J Biochem* 119(2):319–328